ISSN 1674-1056
http://cpb.iphy.ac.cn
http://iopscience.iop.org/cpb
中国物理 B
Chinese Physics
中国物理 Chinese Physics B

Simulation of acoustic fields emitted by ultrasonic phased array in austenitic steel weld

Zhong-Cun Guo(郭忠存)[1,2], Shou-Guo Yan(阎守国)[1], Bi-Xing Zhang(张碧星)[1,2]
Citation: Chin. Phys. B . 2019, 28(11): 114302 . **doi:** 10.1088/1674-1056/ab4d41
Journal homepage: http://cpb.iphy.ac.cn; http://iopscience.iop.org/cpb

What follows is a list of articles you may be interested in

Lamb waves topological imaging combining with Green's function retrieval theory to detect near filed defects in isotropic plates

Hui Zhang(张辉), Hai-Yan Zhang(张海燕), Meng-Yun Xu(徐梦云), Guo-Peng Fan(范国鹏), Wen-Fa Zhu(朱文发), Xiao-Dong Chai(柴晓冬)
Chin. Phys. B . 2019, 28(7): 074301 . **doi:** 10.1088/1674-1056/28/7/074301

Seismoelectric wave propagation modeling in a borehole in water-saturated porous medium having an electrochemical interface

Hao-Ran Ding(丁浩然), Jin-Xia Liu(刘金霞), Zhi-Wen Cui(崔志文), Tribikram Kundu
Chin. Phys. B . 2017, 26(12): 124301 . **doi:** 10.1088/1674-1056/26/12/124301

Seismoelectric wave propagation modeling in a borehole in water-saturated porous medium having an electrochemical interface

Hao-Ran Ding(丁浩然), Jin-Xia Liu(刘金霞), Zhi-Wen Cui(崔志文), Tribikram Kundu
Chin. Phys. B . 2017, 26(12): 124301 . **doi:** 10.1088/1674-1056/26/12/124301

Rayleigh reciprocity relations: Applications

Ju Lin(林巨), Xiao-Lei Li(李小雷), Ning Wang(王宁)
Chin. Phys. B . 2016, 25(12): 124303 . **doi:** 10.1088/1674-1056/25/12/124303

Quantitative damage imaging using Lamb wave diffraction tomography

Hai-Yan Zhang(张海燕), Min Ruan(阮敏), Wen-Fa Zhu(朱文发), Xiao-Dong Chai(柴晓冬)
Chin. Phys. B . 2016, 25(12): 124304 . **doi:** 10.1088/1674-1056/25/12/124304

Simulation of acoustic fields emitted by ultrasonic phased array in austenitic steel weld*

Zhong-Cun Guo(郭忠存)[1,2], Shou-Guo Yan(阎守国)[1,†], and Bi-Xing Zhang(张碧星)[1,2]

[1] *State Key Laboratory of Acoustics, Institute of Acoustics, Chinese Academy of Sciences, Beijing* 100190, *China*
[2] *University of Chinese Academy of Sciences, Beijing* 100049, *China*

(Received 1 September 2019; revised manuscript received 17 September 2019; published online 30 October 2019)

Ultrasonic inspection of austenitic steel weld is a great challenge due to skewed and distorted beam in such a highly anisotropic and inhomogeneous material. To improve the ultrasonic measurement in this situation, it is essential to have an in-depth understanding of ultrasound characteristics in austenitic steel weld. To meet such a need, in the present study we propose a method which combines the weld model, Dijkstra's path-finding algorithm and Gaussian beam equivalent point source model to calculate the acoustic fields from ultrasonic phased array in such a weld. With this method, the acoustic field in a steel-austenitic weld-steel three-layered structure for a linear phase array transducer is calculated and the propagation characteristics of ultrasound in weld are studied. The research results show that the method proposed here is capable of calculating the acoustic field in austenitic weld. Additionally, beam steering and focusing can be still realized in the austenitic steel weld and the beam distortion is more severe in the middle of weld than at other positions.

Keywords: simulation of acoustic field, ultrasonic phased array, austenitic steel weld

PACS: 43.20.+g, 43.35.+d, 43.38.+n **DOI:** 10.1088/1674-1056/ab4d41

1. Introduction

Austenitic steel, as a kind of specific complex material, is welded widely in nuclear power plants and other industries.[1–5] For security reasons, it is of great importance to evaluate the structural integrity of the austenitic steel weld. However, due to the high anisotropy and inhomogeneity, huge difficulties exist when using ultrasound technique to inspect such a structure. Apart from the energy attenuation, the elastic wave will be spited and skewed, which makes the testing results inaccurate. As a result, developing a method to evaluate the acoustic fields inside austenitic steel weld has become an urgent need.

Up to now, a lot of efforts have been made by numerous researchers. Silk[6] first developed a computer model based on ray tracing technique to predict the ray paths in complex orthotropic structures. Ogilvy[7,8] presented a weld model to approximately describe the grain orientation at each position and developed the RAYTRAIM, a commercial software package, based on weld model and traditional ray tracing technique. Spies[9] calculated the acoustic fields emitted from a single transducer in multilayered inhomogeneous anisotropic medium and austenitic steel weld respectively by using multi-Gaussian beam (MGB) model. Ye *et al.*[10] presented a model combining the traditional ray tracing technique and the linear phasing multi-Gaussian beam model to calculate the focused fields produced by a phased array transducer in dissimilar metal welds. Kolkoori *et al.*[11] introduced the ray directivity factor into ray tracing technique and calculated the acoustic fields in specific directions from distributed sources in austenitic steel weld. Simulation results were validated with the results obtained from two-dimensional (2D) elastodynamic finite integration technique (EFIT) and experiments. Although the traditional ray tracing technique is a powerful tool for determining the ray path, it must be run many times if the number of target points is large, which will increase the computation time. In such a situation, Nowers Oliver *et al.*[12,13] first adopted the Dijkstra's algorithm and A* algorithm which have been widely used in computer science for finding the shortest path to predict the ray paths in austenitic steel welds efficiently. And, it is worth mentioning that the Dijkstra's algorithm,[14] as a novel ray tracing technique, can be used to obtain the ray paths from one source to any number of target points in one run. However, such an algorithm can only be used to determine the ray path but not to calculate the amplitude of acoustic field.

For the calculation of acoustic fields in frequency domain, the multi-Gaussian beam (MGB) model, based on the superposition of several (10–15) special Gaussian beams, has been widely used by numerous researchers[15–19] and considered as the most efficient method, especially in multiple medium. However, due to the assumption of paraxial approximation, when it comes to phased array, this method will lose accuracy if the steering angle becomes too large.[20] For this reason, some efforts have been made to solve this problem. Zhao[21,22] expressed the distance factor in terms of several approximate terms and proposed a nonparaxial multi-Gaussian

*Project supported by the National Natural Science Foundation of China (Grant Nos. 11474308, 11574343, and 11774377).
†Corresponding author. E-mail: yanshouguo@mail.ioa.ac.cn
© 2019 Chinese Physical Society and IOP Publishing Ltd

beam model. Huang[23–25] introduced 2 modification factors into the MGB model including linear phasing and directivity function and developed the LPMGB model. Furthermore, Schmerr[15] combined the point source superposition model and Gaussian beam method, and finally developed the Gaussian beam equivalent point source (GBEPS) model. In this model, the surface of each transducer is considered as the superposition of several point sources and each point source emits spherical wave into medium. Through substituting a specific Gaussian beam for spherical wave and rotating the coordinate system to make each field point be on the main axis of Gaussian beam, the limitation of paraxial approximation can be eliminated. In view of this, the GBEPS model is used here to simulate the acoustic fields emitted by ultrasonic phased array in austenitic steel weld.

Therefore, in this work, for evaluating the acoustic field in weld, a systematic method combining with the weld model for describing grain orientation inside austenitic steel weld, the Dijkstra's algorithm for obtaining ray paths, and the Gaussian beam equivalent point source (GBEPS) model[15] for calculating the amplitude of displacement is introduced and discussed. In addition, as a simulation example, the case of steel-weld-steel with linear phased array transducer is considered and the focusing and steering fields are calculated and analyzed by using the proposed approach.

2. Model for simulating acoustic fields in austenitic steel weld

2.1. Weld model

Generally, the austenitic steel weld is a kind of anisotropic and inhomogeneous material. In the formation of the weld, crystalline grains grow along the maximum thermal gradient when cooling,[3] which causes the coarse grains with different orientations: such a formation process is different from that of isotropic material. As a result, while traveling through such a material, the ultrasound will be steered and distorted by these grains, which means that the determination of grain orientations plays an important role in studying the propagation of ultrasound in austenitic steel weld. In this paper, the weld model presented by Ogilvy[7] is adopted, which gives a mathematical empirical function to describe the local grain orientations of the weld. The form of function is given as

$$\theta(x,z)=\begin{cases}\arctan\left(\dfrac{-T(D+z\tan\alpha)}{x^{\eta}}\right), & x\geq 0,\\ \arctan\left(\dfrac{T(D+z\tan\alpha)}{(-x)^{\eta}}\right), & x<0,\end{cases} \tag{1}$$

where θ is the grain orientation with respect to the x axis, T is the slope of the grain axis at the fusion face, D is the half width of the weld root gap, η is the rate of change of orientation throughout the weld, and α is the fusion face angle [Fig. 1(a)]. It can be seen from Eq. (1) that only 2D situation (xoz plane) is considered, which means that the three-dimensional (3D) austenitic steel weld is regarded as a transversely isotropic medium. In addition, using Eq. (1), the virtual boundary, on which the nodes have the same grain orientation, can alsobe calculated.

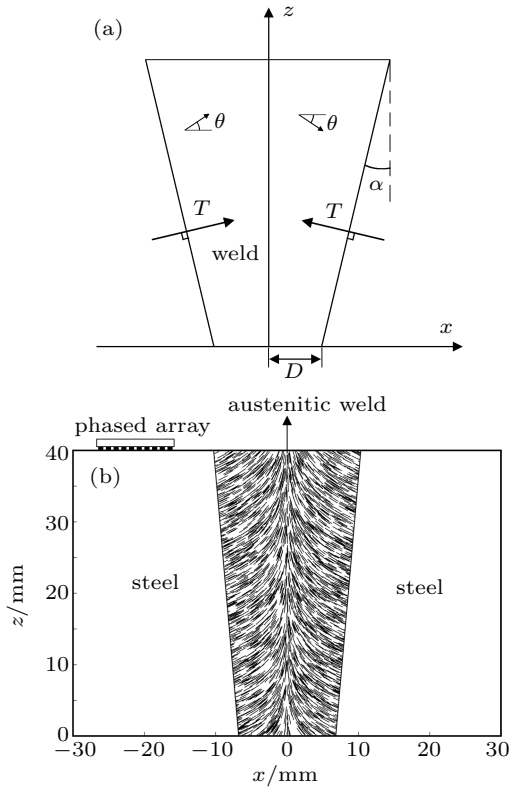


Fig. 1. Austenitic steel weld model.

Figure 1(b) shows the simulation model used in this study, where the austenitic steel weld is surrounded by an isotropic steel material, and the phased array is placed on the surface of the steel. It also shows the grain orientations of the weld calculated by Eq. (1), where $T=0.3$, $\eta=0.85$, $D=7.5$, and $\alpha=5^{\circ}$. In this model, the transversely isotropic type-316 austenitic steel weld metal[12] is used for numerical calculation and its density and material elastic properties are shown in Table 1.

As a matter of fact, the phase velocity c is generally different from group velocity $\boldsymbol{V}$ in anisotropic medium and the energy always propagates along the direction of group velocity. Therefore, the determination of group velocity is also important here. According to the theory of solid acoustics,[11] the relationship between group velocity $\boldsymbol{V}$ and phase velocity c is expressed as

$$V_j=\frac{C_{ijkl}l_k u_i u_l}{\rho c}, \tag{2}$$

where C_{ijkl} are the matrix stiffness constants, l_k is the direction cosine of wave vector, u_i is the particle displacement, ρ is the density of material, and $i, j, k, l=1, 2, 3$. Therefore, to obtain the phase velocity and group velocity in the weld, bond matrix

transformation[11] is used to transform the elastic constant into local crystal axis coordinate according to the grain orientation at each node.

Table 1. Material properties for transversely isotropic type-316 austenitic steel weld metal.

Material parameter	Value	Unit
ρ	8120	kg/m^3
c_{11}	263	GPa
c_{12}	98	GPa
c_{13}	145	GPa
c_{33}	216	GPa
c_{44}	129	GPa
c_{66}	82.3	GPa

Figure 2 shows the slowness curve of quasi-P (qP) wave in austenitic steel in the *xoz* plane when the crystal axis is parallel to the *z* axis. According to the relationship between group velocity, phase velocity and slowness curve, it can be discovered from Fig. 2 that the group velocity and phase velocity are different except in the pure mode directions (0°, 45.26°, and 90°). When the acoustic beam is incident into austenitic steel, although its phase velocity direction conforms to snell's law, the energy of the acoustic beam propagates along the direction of group velocity. Therefore, it is very complicated to calculate the sound field in the austenitic steel weld with changing grain orientation.

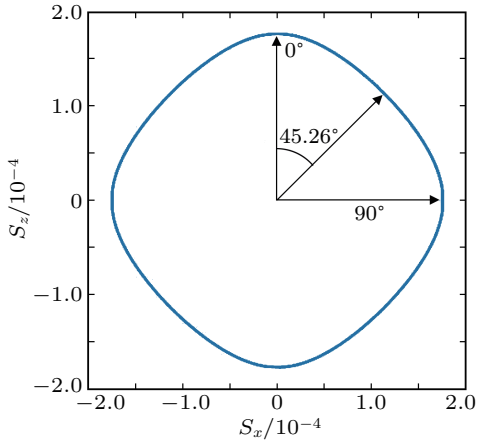


Fig. 2. Slowness curve of qP wave with pure mode directions (0°, 45.26°, and 90°) in austenitic steel weld.

2.2. Calculation of acoustic fields in weld

Consider a linear phased array with N elements. Each element is divided into Q segments which are tiny enough to be regarded as point sources emitting spherical wave. According to the GBEPS model, such a spherical wave at each field point is approximated as a specific Gaussian beam. And the particle velocity in the $M+1$ medium, $\boldsymbol{v}_{M+1}$, generated by the n-th element with Q segments, is given as[15]

$$\boldsymbol{v}^n_{M+1}(\omega) = v_0 A \sum_{q=1}^{Q} \left\{ D^q_R \boldsymbol{d}^q_{M+1} \frac{\sqrt{\det\left[M^q_{M+1}\left(s^q_{M+1}\right)\right]}}{\sqrt{\det\left[M^q_{M+1}(0)\right]}} \times \left[\prod_{m=1}^{m=M} T^q_m \frac{\sqrt{\det\left[M^q_m\left(s^q_m\right)\right]}}{\sqrt{\det\left[M^q_m(0)\right]}} \right] \times \exp\left[\mathrm{i}\omega \sum_{m=1}^{M+1} \frac{s^q_m}{c_m} \right] \right\}. \quad (3)$$

In Eq. (3), v_0 is the velocity amplitude of the Gaussian beam on the element face; D_R is the directivity function; $\boldsymbol{d}^q_{M+1}$ is the unit polarization vector; M^q_m, a 2×2 matrix, related to the density, the wave speed, the incident angle, and the refracted angle in the M-th medium, can be obtained by using the ABCD matrix method;[23] T_m is the plane wave transmission/reflection coefficient between M-th and $(M+1)$-th mediums, and can be calculated by solving the Christoffel equation and slowness surface;[13] s_m is the propagation distance of group velocity (rather than phase velocity) in the M-th medium along the ray path; c_m is the phase velocity in the M-th medium, which can be obtained by solving the Christoffel equation.

From Eq. (3), it can be discovered that the expression of particle velocity contains two parts: amplitude and phase, and both of them in the i-th layered medium can be calculated by those in the $(i-1)$-th layered medium. Additionally, the determination of the ray path from group velocity is of great importance for calculating the wave fields. Therefore, the Dijkstra's algorithm,[17] a kind of path finding method in computer science, is adopted to obtain the ray path which has the shortest propagation time of group velocity. Based on this, a method of combining weld model, Dijkstra's algorithm and GBEPS model is presented here to calculate the acoustic fields in austenitic weld.

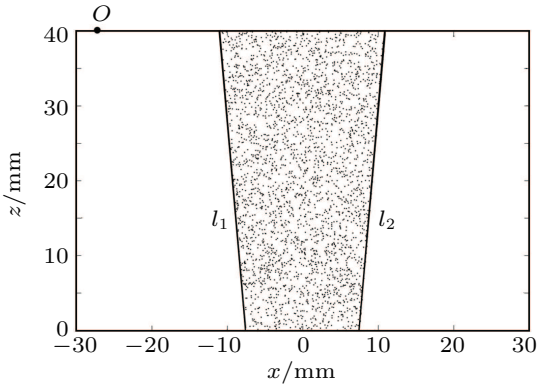


Fig. 3. Numerical nodes distributed randomly in austenitic weld.

According to the Dijkstra's algorithm, a large number of nodes are distributed randomly in the austenitic weld and on the interfaces (l_1 and l_2) (Fig. 3), which means that the acoustic fields and ray paths in austenitic weld are represented by these nodes. Define d_r as the step distance of Dijkstra's algorithm. In Fig. 4(a), the amplitude and phase of N_1 on the interface l_1 can be simply calculated through Eq. (3). And then, the main steps involved in calculating ray path and acoustic field in the weld are as follows.

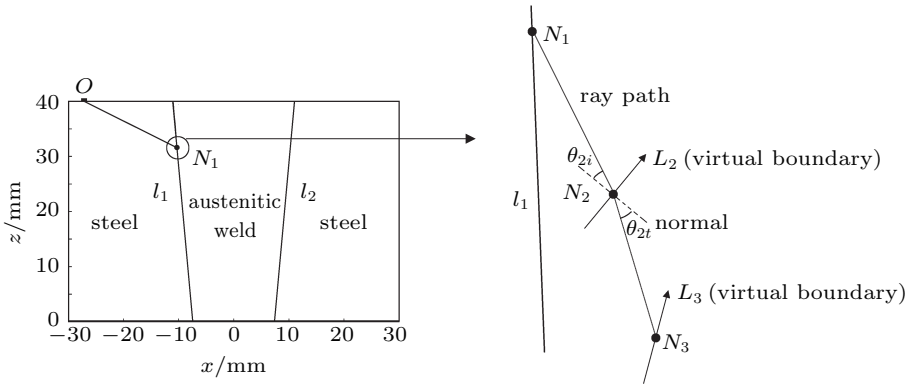


Fig. 4. Model for determinining ray path and acoustic field of node.

(i) Choose a current node N_1 on the interface l_1 [Fig. 4(a)] and obtain the adjacent nodes whose distances are less than dr from N_1.

(ii) With the known grain orientations at these adjacent nodes, calculate the phased velocity and group velocity corresponding to the propagation directions from N_1 to them. And then, the propagation time of group velocity can be obtained., on the assumption that the materials between N_1 and its adjacent nodes are homogeneous anisotropic medium.

(iii) Find the node N_2 which has the shortest propagation time and define it as the new current node [Fig. 4(b)]. Using the vectors ON_1, N_1N_2 and interface l_1 to calculate the incident, refracted angle θ_{1i} and θ_{1t}, and transmission coefficient T_1 at l_1 corresponding to group velocity at N_1. And then, the amplitude and phase of particle velocity at N_1 can be calculated using Eq. (3).

(iv) Calculate the vector of virtual boundary L_2 at current node N_2 using Eq. (1) and draw the normal. Find the next current node N_3 corresponding to N_2.

(v) Calculate the incident, refracted angle θ_{2i}, θ_{2t}, and transmission coefficient T_2 at N_2.

(vi) Using Eq. (3), calculate the amplitude and phase of $\boldsymbol{v}_2$ at N_2 according to that of N_1.

(vii) Repeat Steps (iv)–(vi) until all of nodes in weld are calculated.

After the above algorithm is done, the acoustic fields of all the nodes in the weld, generated by one element of transducer, are calculated. When the phased array transducer with N elements is used, the acoustic fields can be calculated by superposing the results from all elements with proper time delay, which is expressed by

$$\boldsymbol{v}_{M+1} = \sum_{n=1}^{N} \boldsymbol{v}_{M+1}^{n} \exp(\mathrm{i}\omega \cdot \Delta t_n). \tag{4}$$

3. Simulation results and analysis

To demonstrate the presented method, the radiated acoustic fields emitted by a linear phased array transducer in steel-austenitic steel weld-steel structure [Fig. 1] are calculated. In this section, the width of the element is 0.2 mm while the distance between centroids of adjacent elements is 0.25 mm. Each element is assumed to be in harmonic vibration with a frequency of 8 MHz. The density of steel is 7850 kg/m^3 and the longitudinal wave velocity and shear wave velocity in steel are 5800 m/s and 3200 m/s respectively. The parameters of weld are given in Table 1. In addition, for simplicity, during numerical simulation the wave attenuation and scattering are not considered just as done in other research.[10]

Figure 5 shows the ray paths of longitudinal wave, calculated by the Dijkstra's algorithm, travelling from the point source O to several target points in steel and austenitic steel weld. From the result, it can be discovered that the ray path is straightline in steel and is distorted in weld.

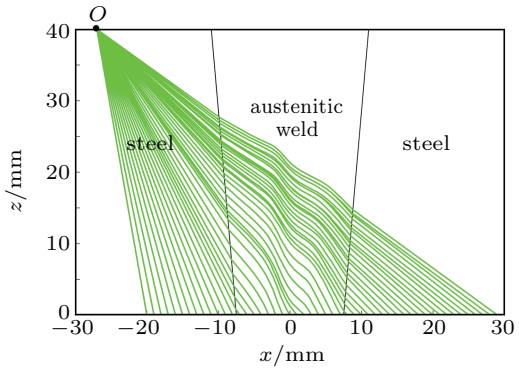


Fig. 5. Ray path calculated by Dijkstra's algorithm.

Figures 6(a)–6(d) show the acoustic fields emitted by ultrasonic phased array with steering angle (in the steel) (a) 0°, (b) 30°, (c) 45°, and (d) 60° respectively. By comparing the propagation behavior of ultrasound in steel with that of weld, some differences can be discovered. In Fig. 6(a), the ultrasonic beam emitted by phased array without time delay propagates along a straight line because of isotropic medium. But in Fig. 6(b), the steered beam starts to be refracted into weld and it almost propagates along a straight line at the beginning. But when the steered beam arrives at the middle of the weld, beam distortion occurs obviously as shown in Figs. 6(c)–6(d), which show the great difference between the ultrasound propagation in steel and that in weld. In the weld, the grain orientation

varies continuously and the group velocity differs from that from each direction. It can be assumed that the steered beam is refracted many times in the weld, which causes the beam distortion.

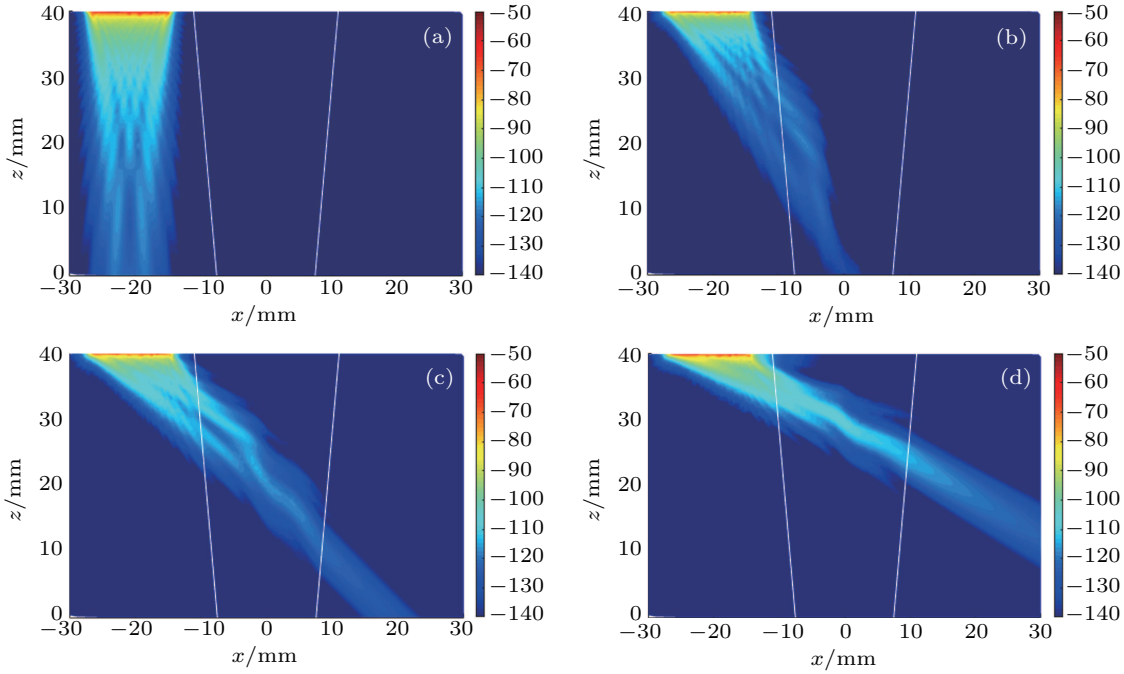


Fig. 6. Acoustic fields with steering angle (a) 0°, (b) 30°, (c) 45°, and (d) 60°.

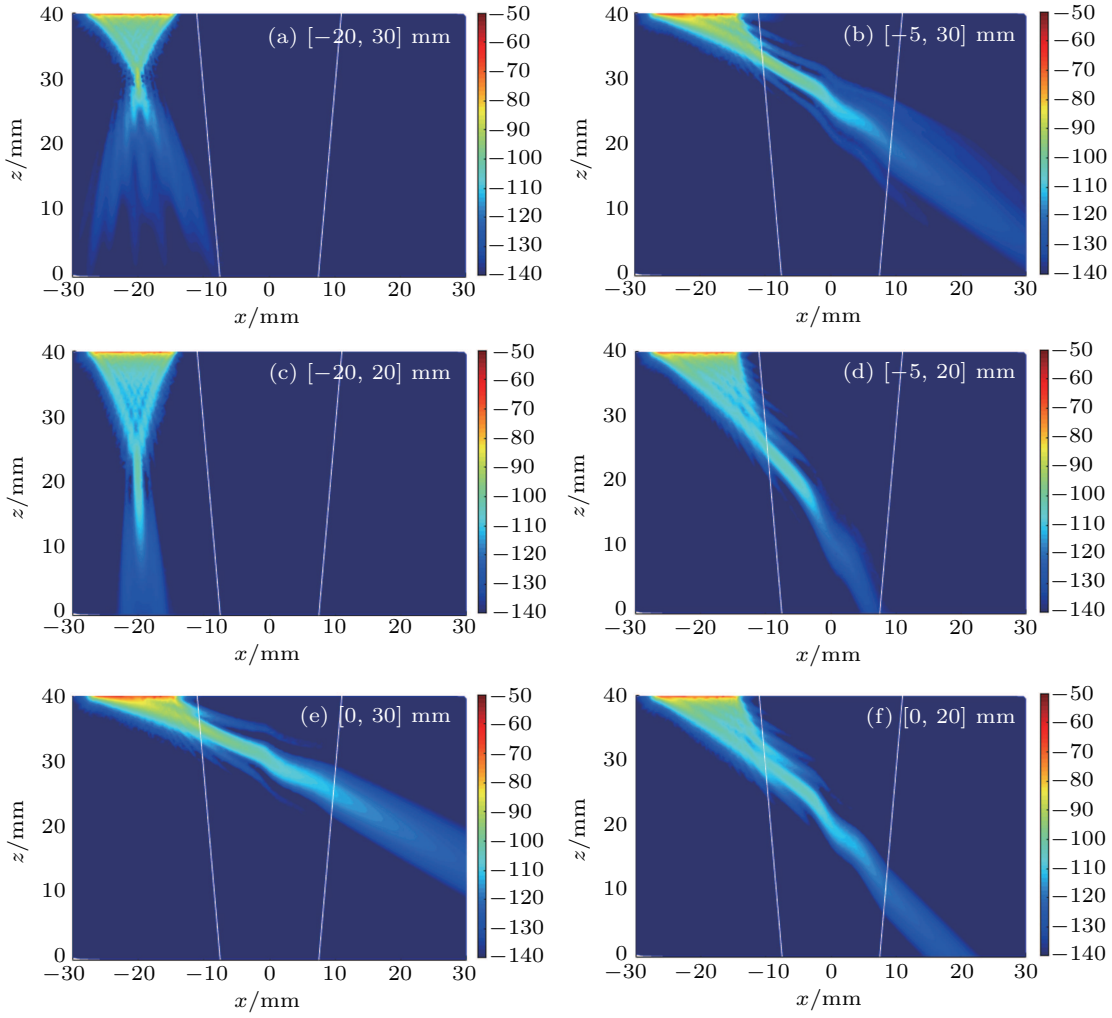


Fig. 7. Acoustic fields focused at several points: (a) [−20,30] mm, (b) [−5,30] mm, (c) [−20,20] mm, (d) [−5,20] mm, (e) [0,30] mm, (f) [0,20] mm.

To make acoustic wave focus at a specific point, time delays of all elements should be obtained at first by using Dijkstra's algorithm. Figure 7 shows the longitudinal wave fields focused at (a) [−20, 30], (b) [−5, 30], (c) [−20, 20], (d) [−5,20], (e) [0, 30], and (f) [0, 20] mm respectively. When the acoustic field is focused into steel, the focal spot becomes longer and wider as the focal distance increases, which is similar to the results calculated by Song.[26] As shown in these results, with the presented simulation method, the beam focusing is also realized in weld and it can be discovered that the focal spot is generally wider in weld than in steel, partly because of larger steering angle in weld, and also partly for the dispersion of energy in weld as mentioned above. As expected, comparing Fig. 6 with Fig. 7, the amplitude from focused field is indeed much higher than that from steering field at focal point. In addition, in Figs. 7(e) and 7(f), none of the actual focal points is the same as predetermined focal points although the wave fronts arrive at the predetermined focal point simultaneously, which shows the focusing limitation of the phased array. Such a discrepancy between actual focal point and predetermined focal point can be solved through improving the frequency and increasing the number of elements.

At present, during setting the detection parameters and image processing, the ultrasonic detection of welds is still generally based on the weld model under the assumption of isotropic medium. In practice, however, the propagation path of sound wave in the real austenitic stainless steel welds is deflected and bent as shown in Figs. 6 and 7. Obviously, such an assumption will lead the application of current detection schemes to be questionable. In the past, due to the lack of reliable weld model for simulation, one did not have an in-depth understanding of these problems. In the following, this problem will be analyzed through the numerical simulation. In order to match the actual probe, the width of the element is taken to be 0.8 mm while the distance between centroids of adjacent elements is adopted as 1.0 mm. Each element is assumed to be in harmonic vibration with a frequency of 8 MHz, and the parameters of media and weld structure are the same as those mentioned above.

Firstly, for a real austenitic stainless steel weld, if the isotropic medium model is used to simplify the calculation, the ray paths and time delays of phased array will be obtained easily, but the actual acoustic beam cannot accurately focus on the target point. Figure 8 shows the focused acoustic fields calculated by the proposed method and the method under the assumption of isotropic medium respectively. The structural parameters of the weld are the same as those mentioned above. In order to display the characteristics of focused acoustic fields more clearly, the drawing display range is limited between [−60, −80] dB. Figures 8(a) and 8(c) are the results obtained by proposed method with the presupposed focal points at [0, 10] mm and [0, 20] mm. Figures 8(b) and 8(d) show the results from traditional isotropic model with the same focal points. As can be seen, when the isotropic model is used, the actual focal point deviates from the preset focus position farther (to the upper left) than the present model. It should be noted that the actual focal points in Figs. 8(a) and 8(c) are also in the front of the preset focus, but this is a common feature of the focused acoustic field in phased array, which is caused by the diffraction of acoustic waves and can be predicted and improved by adjusting the parameters such as frequency and spacing of array elements. The offsets in Figs. 8(b) and 8(d) are due to the fact that the weld structural parameters (T, η, D, and α) are not introduced into the calculation of time delays. It is also found that the amplitude and offset of focused beam change with focal point and structural parameters. However, under the isotropic model, these changes are unpredictable, which would lead to the false detection and mis-detection in practice. In contrast, the simulation model proposed in this paper can help us to detect the propagation characteristics of sound beam clearly, and has a guiding role in actual detection.

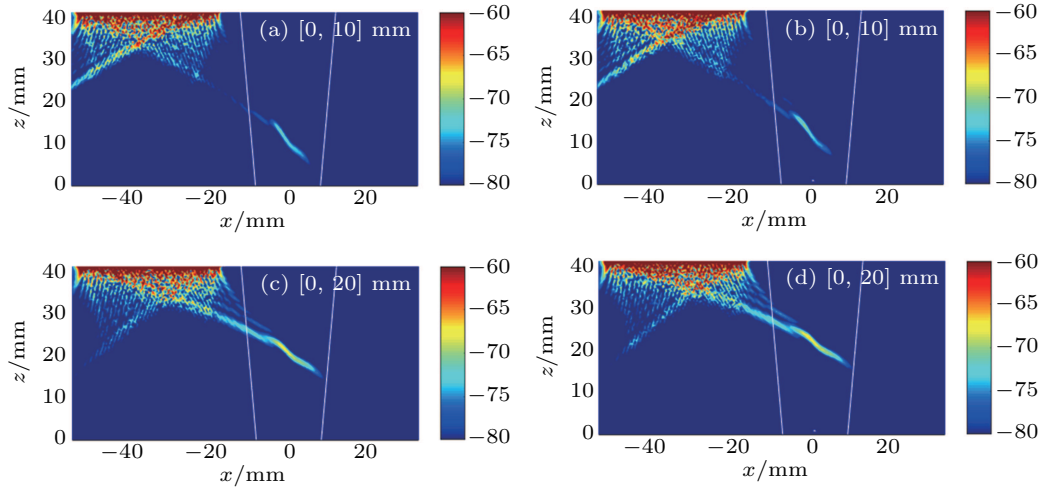


Fig. 8. Comparison among focused sound fields in anisotropic weld model (Ogilvy) under different delay rules. Delays are calculated by using ((a), (c)) proposed method and ((b), (d)) isotropic model.

In addition, in the process of defect imaging, such as time reversal focusing imaging, the actual delayed echo data are affected by the inhomogeneous anisotropy of weld, but such an effect cannot be reconstructed in the isotropic medium model, which will lead to inaccurate defect imaging results. At this time, more accurate weld simulation model is needed to reconstruct the echo data, and the model and algorithm proposed here can be used to improve the imaging accuracy. Figure 9 shows a simplified simulation result of this problem. The time delays from Ogilvy weld model with focal point at [0, 20] mm are obtained and used to simulate the actual delayed echo data. The focused sound fields are calculated under the present model and the isotropic medium model respectively to analyze the imaging results. It can be seen from Fig. 8 that compared with the results from the isotropic medium model, the results from the proposed model indicate that the actual focal point is very close to the preset focal point, and the beam energy is highly concentrated, which demonstrates better imaging accuracy from the proposed model.

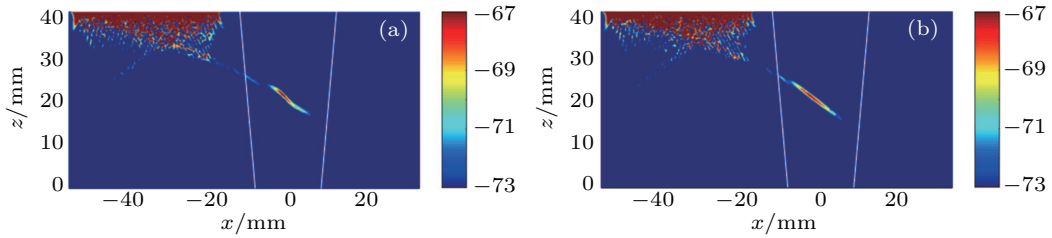


Fig. 9. Focused sound fields with the same time delay in (a) Ogilvy weld model and (b) isotropic weld model.

4. Conclusions

A systematic method combining with weld model, Dijkstra's algorithm and Gaussian beam equivalent point source model is presented and allows the calculation of acoustic fields generated by phased array transducer in austenitic steel weld. As a simulation example, the case of steel-austenitic steel weld-steel with linear phased array is considered, in which, the longitudinal acoustic fields with different time delays are calculated and beam steering and focusing are realized. As the example illustrates, useful information including ray path, particle velocity amplitude and propagation characteristics in austenitic steel weld can be obtained, which demonstrates the capability of the proposed method. Simulation results show the propagation behavior of ultrasound through austenitic steel weld and also indicate that the ultrasound is distorted and skewed severely in the middle of the weld. Finally, the problems that may be caused by the isotropic theory in the actual austenitic weld inspection are analyzed. These results present theoretical support for actual ultrasound testing.

Acknowledgement

One of the authors, Zhong-Cun Guo, worked under the support from the UCAS Joint PhD Training Program and the Fraunhofer Institute for Ceramic Technologies and Systems IKTS in Germany, for which the author would like to express his heartfelt thanks.

References

[1] Kupperman D S and Reimann K J 2005 *IEEE Trans. Sonics & Ultrason.* **27** 7
[2] Halkjær S, Sørensen M P and Kristensen W D 2000 *Ultrasonics* **38** 256
[3] Liu Q W and Wirdelius H 2014 *Modelling and Simulation in Engineering* **2014** 637476
[4] Fereidooni B, Morovvati M R and Sadough-Vanini S A 2018 *Ultrasonics* **88** 137
[5] Lhuillier P E, Chassignole B, Oudaa M, *et al.* 2017 *Ultrasonics* **78** 40
[6] Silk M G 1981 *Ultrasonics* **19** 208
[7] Ogilvy J A 1985 *Non-Destructive Test. Int.* **18** 67
[8] Ogilvy J A 1986 *Ultrasonics* **24** 337
[9] Spies M 2000 *NDT & E Int.* **33** 155
[10] Ye J, Kim H J, Song S J, Kang S S, Kim K and Song M H 2011 *Ndt & E Int.* **44** 290
[11] Kolkoori S R, Rahman M U, Chinta P K, Ktreutzbruck M, Rethmeier M and Prager J 2013 *Ultrasonics* **53** 396
[12] Nowers O, Duxbury D J, Zhang J and Drankwater B W 2014 *Ndt & E Int.* **61** 58
[13] Nowers O, Duxbury D J and Drinkwater B W 2016 *Ndt & E Int.* **79** 98
[14] Dijkstra E 1959 *Numer. Math.* **1** 269
[15] Schmmer L W 2015 *Fundamentals of Ultrasonic Phased Arrays* (New York: Springer) pp. 138–146
[16] Wen J J and Breazeale M A 1988 *J. Acoust. Soc. Am.* **83** 1752
[17] Duan X M, Zhao X Y and Sun H F 2014 *Acta Phys. Sin.* **63** 014301 (in Chinese)
[18] Guo W J, Chen Y X, Jin Y and Wang Z B 2013 *Appl. Acoustics* **32** 354
[19] Han P, Wang Z B and Chen Y X 2010 *Transducer Microsyst. Technol.* **29** 22 (in Chinese)
[20] Park J S, Song S J and Kim H J 2006 *Solid State Phenom.* **110** 163
[21] Zhao X Y, Gang T and Zhang B X 2008 *Acta Acoustic* **33** 475 (in Chinese)
[22] Zhao X Y and Gang T 2009 *Ultrasonics* **49** 126
[23] Huang R J and Schmerr L W 2005 *Res. Nondestr. Eval.* **16** 143
[24] Huang R J, Schmerr L W and Sedov A 2007 *Res. Nondestr. Eval.* **18** 193
[25] Huang R J, Schmerr L W and Sedov A 2007 *Am. Inst. Phys.* **894** 751
[26] Song S J and Kim C H 2002 *Ultrasonics* **40** 519